

# Effective Solid Angle Model and Monte Carlo Method: Improved Estimations to Measure Cosmic Muon Intensity at Sea Level in All Zenith Angles

Junghyun Bae <sup>a</sup>, Stylianos Chatzidakis <sup>a</sup>, Robert Bean <sup>a</sup>

<sup>a</sup> School of Nuclear Engineering, Purdue University, West Lafayette, IN 47906, United States

## ABSTRACT

Cosmic muons have higher energy and are more penetrative compared to induced radiation typically used for imaging. Due to these properties, cosmic muons can be used for imaging in many industries with large and dense objects, including imaging uranium fuel for nuclear security and safeguards. Cosmic muon intensity varies along the incident angle (zenith angle,  $\varphi$ ), and it is known to follow a cosine-squared at sea level such that  $I(\varphi) = I_0 \cos^2 \varphi$ . The low overall intensity means that muon imaging will take a longer time to acquire statistically meaningful counts, whether for muon scattering or absorption tomography, compared to induced radiation systems. Therefore, high-energy particle simulations like GEANT4 are often used to enhance and guide measurement studies. However, unlike in the simple theory, the measurable cosmic muon count rate changes upon detector geometry and configuration. It is possible therefore to mislead the experimenter as to actual muon count rates and imaging construction time required for practical applications. Here we show the effective solid angle model and Monte Carlo method, which were developed based on the cosine-squared law coupled with detector geometry, estimate the experimental results more precisely than the simple cosine-squared model. An effective solid angle model must consider the actual measurable solid angle made by the physical geometry of and their alignment when measuring the passage of cosmic muons through the system. The solid angle calculated from the detector geometry is coupled with the cosine-squared law and it is introduced as an effective solid angle. The simple cosine-squared model has high error compared to experimental values for high zenith angles ( $\varphi \geq 60^\circ$ ); our results demonstrate that the new model properly estimates experimental measurements at all zenith angles. Enhanced estimation at high zenith angles allows us to exploit cosmic muon horizontally for muon tomographic applications. We anticipate our methods will enhance the ability to estimate actual measurable cosmic muon count rates in proposed imaging applications by reducing the gap between simulation and measurement results. This will increase the value of modeling results and improve the quality of experiments and applications in muon detection and imaging.

\* **Keywords:** Effective solid angle; Monte Carlo Method; Cosmic Muons; Muon Tomography; NaI(Tl) Scintillation Detectors

## 1. Introduction

Muon is the most abundant cosmic ray particle on Earth. At sea level, about  $10,000/\text{m}^2\text{min}$  of muons reach the earth [1]. It is generally produced from pion decay,  $\pi^\pm = \mu^\pm + \bar{\nu}_\mu$  (or  $\nu_\mu$ ) in the atmosphere and it has a mean lifetime of 2.2  $\mu\text{sec}$ . Muon is an electron-like lepton but 207 times heavier than electron [2]. High energetic and penetrative muons enable to be used for imaging of large and high-density materials that is difficult using typical active interrogation radiation. For example, the penetration depth of 3 GeV muon in water is greater than 10 meters. Cosmic muon tomography is initially devised by Borozdin et al. [3] and it is widely used in geotomography [4]–[7], cargo scanning [8]–[12], and nuclear nonproliferation and safeguard through spent nuclear fuel scanning [13]–[19]. In muon tomography, it is important to understand the types of physical interactions between incident cosmic muons and materials of interest in the system. Because it is not able to observe muon interactions directly, we statistically estimate inside material via imaging reconstruction algorithm using vector information from incoming and outgoing muons [20]–[22]. In other words, it is essential to obtain a statistically meaningful amount of data for fine imaging reconstruction. Although large detector or long-time measurement enables us to obtain significant muon counts, a proper balance between size, time and image quality should be considered. To find the proper balance, we should know actual measurable muon counts. Unlike active interrogation radiation, muon tomography entirely depends on cosmic muon intensity because it is difficult to produce muons for imaging purposes. Because cosmic muon intensity is lower, Monte Carlo simulation like GEANT4 is often used to manipulate intensity or time in many studies [23]–[25]. Physical interactions between high-energy muons and materials are well established using simulation while there is a lack of information on how traveling muon is recorded after interactions in the detector. In practice, a measurable muon count varies upon types of detector, detector geometry, and its configuration. Therefore, a new model considering detector figures is necessary to estimate actual measurable muon counts. Cosmic muon intensity,  $I$ , varies along the zenith angle,  $\varphi$  and it is known to follow a cosine squared, such that  $I(\varphi) = I_0 \cos^2 \varphi$ . However, many experimental results have shown that this relation is not valid at high zenith angles. Specifically, the cosine-squared model overestimates actual muon counts at high zenith angles, whilst it underestimates counts at low zenith angles [26]. To improve this model, we propose the effective solid angle model and Monte Carlo method, which were developed based on the cosine-squared law coupled with the physical dimension of detector. An effective solid angle model must consider the actual measurable solid angle made by the physical geometry of the detectors and their alignment when measuring the passage of cosmic muons through the system. In our experiment, two NaI(Tl) scintillation detectors connected to coincidence logic gate are installed to measure incident cosmic muons at seven different zenith angles. Detectors measure cosmic muons for 24 hours to minimize the count variance upon the time in a day [27]. At all zenith angles, it estimates the experimental results more precisely than the simple cosine squared model. Particularly, the estimation ability is improved at high zenith angle ( $\varphi \geq 60^\circ$ ). Our model will improve the value of modeling results and increase the quality of experiments and applications in muon tomography.

## 2. Materials and Methods

### 2.1. NaI (TI) Scintillation Detector System

Sodium Iodide (NaI) scintillation crystal and photomultiplier tube (PMT) are encapsulated in the thin (0.508 mm) aluminum light shielding. The NaI crystal, located at the bottom of the aluminum housing, has a dimension of 50.8 mm diameter (2 inches) and 50.8 mm height (2 inches). The photomultiplier base with preamplifier is connected as a module. The detailed specifications of two NaI crystals, PMTs, and preamplifiers are summarized in Table 1.

Table 1 Specifications of Sodium Iodide scintillators, preamps, and PMT of two detectors [28], [29]

NaI (TI) Scintillation detectors			Photomultiplier Base with Preamplifier	
Labeled	Detector I	Detector II	Model	ORTEC 276
Serial number	AA-5876-I	AA-5879-I	PMT stages	10
Manufacturer	BICRON		Conversion Gain	$10^5 - 10^6$
Model	2M2/2		Output Rise Time	< 100 nsec
Scintillator	NaI (TI)		Output Fall Time	$\tau = 50 \mu\text{sec}$
Density	3.67 [g/cm <sup>3</sup> ]		Output Noise	< 50 $\mu\text{V}$
Crystal dimension	Diameter = 50.8 mm Thickness = 50.8 mm		Dimensions	Diameter = 56 mm Height = 102 mm
Yield	38,000 [Photons/MeV]			

### 2.2. Experiment Set up

Two scintillation detectors are placed in a line facing each other. With this set up, we can discriminate muon signals from other particles' by taking advantage of the high penetrative figure. Configuration of two-scintillation detector set up and couple of incoming muon tracks are shown in Fig. 1. High-energy muons reached detectors at sea level have average energy of 4 GeV [30]. Incoming cosmic muon releases about 7 MeV/cm within detectors by interacting with NaI crystal lattice [31]. Interactions result in emitting numerous scintillation photons depending on particle energy. Scintillation photons produce the photoelectrons and they are multiplied through the PMT with high voltage supplier. The interactively transferred energy from muon to the scintillation crystals ultimately results in the signals from the preamplifier. The higher energy particle comes in, the larger signal output is recorded. Preamplifier output signals are transferred to the amplifier to reshape the pulse. By passing through the amplifier, Gaussian shaped pulse with thinner width is made. Gain of amplifier is set as minimum ( $0.5 \times 5$ ) because the energy transferred from the high-energy muon is significant and to suppress the noise. The discriminator level of single channel analyzer (SCA) is set as maximum or 10 V to filter out the suppressed noise and signals from other low-energy particles. Both detector systems operate independently, but they share the coincidence logic gate. The generated signals from both detector system's SCAs enter the coincidence logic gate, which only counts the signals occurred within 500 ns beyond peak detect [32]. By using coincidence logic gate, we can free

from the randomly appearing signals. We can only measure signals triggered at both detector system coincidentally. Measurable solid angle range is much narrower using two-detector system instead of one while most of noises can be eliminated because two independent detection system has less than 1% chance to measure noise coincidentally [33]. In addition, we filtered out the signals from other types of radiation by minimizing gain of amplifier and maximizing SCA discriminator level. Consequently, we can selectively detect cosmic muons within the measurable solid angle, which determined by the size of crystals, distance, and their alignment. The apparatus block diagram of described two-scintillation detector set up is shown in Fig. 2.

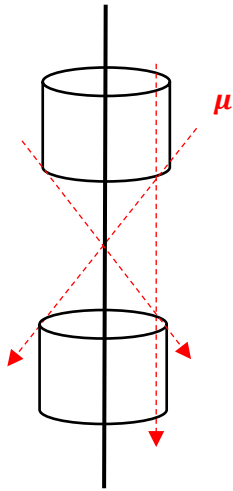


Fig. 1. Schematic diagram of measurable range and track of cosmic muon in two-scintillation detector set up.

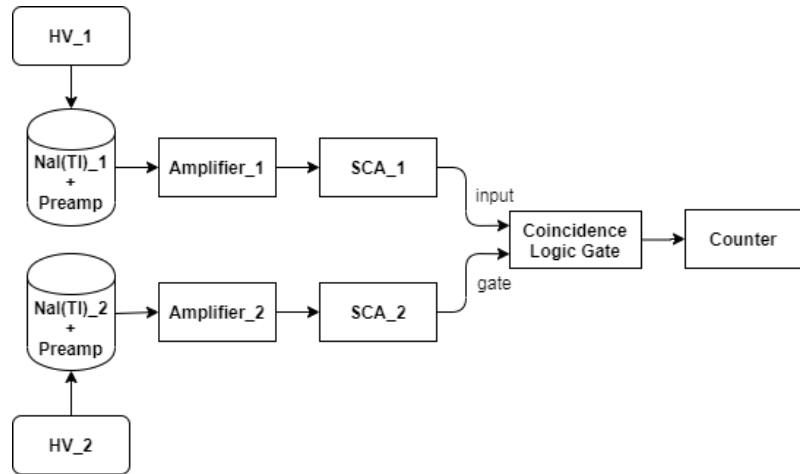


Fig. 2. Apparatus block diagram of two-scintillation detector set up. It shows the two independent scintillation detector systems send signals to the coincidence logic gate for measurements.

### 2.3 Signal Output Analysis

Signal shape from the preamplifier has an instant rising and prolonged tail. The amplitude of the pulse is proportional to the incoming charges from the PMT. The preamplifier pulse shape depends on many factors such as incoming radiation energy, applied high voltage, PMT and crystal properties. We suppose that two large pulses from the preamplifier recorded simultaneously, which installed in the two independent NaI scintillation detectors systems are originated from the high-energy cosmic muon because almost none of other types of radiation can produce large pulses in the ambient condition at sea level. The pulses from the amplifier are easily saturated (12.2 V) in our system since the preamplifier signals is larger enough before entering the amplifier even though the amplifier gain is set as minimum ( $\times 2.5$ ). The amplifiers successfully reshape the pulse from the long-tailed triangle to the Gaussian and record them. Two squared pulses generated from the SCAs, which are survived from the maximum SCA window level (10 V) are recorded. SCA pulse width of 500 nsec is implying that it has rare chance to measure random noise from two independent system unless they are generated from the high-energy particles.

### 3. Analytical Model

To quantify measurable cosmic muon counts described in Fig 3, projected plane angle is firstly introduced (Fig. 4). It is a two dimensional projected plane of detectable solid angle at point where muon interacts with scintillator. Once projected plane angle of detection system is determined, it can be applied to develop the effective solid angle model.

#### 3.1. Projected Plane Angle

Projected plane angle is a possible detectable plane angle in a two-detector system denoted as  $\theta$  and shown in Fig 3. Due to the physical geometry and position, the projected plane angle within a detector surface varies along the distance from the centerline of detectors, which denoted as  $r$ . For different geometries, equivalent diameter ( $D_e$ ) of crystal plane can be used.

$$D_e = 2\sqrt{Area/\pi} \quad (1)$$

One example is described in Fig. 3 showing detectable muon track range that passes one point (solid circle) and its corresponding projected plane angle,  $\theta$ .

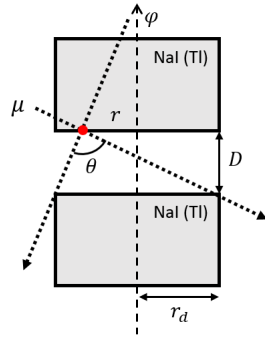


Fig. 3 Detectable cosmic muon track with detecting medium at a random point (solid circle) of the upper detector. Included angle of measurable muon track range is denoted as projected plane angle,  $\theta$ .

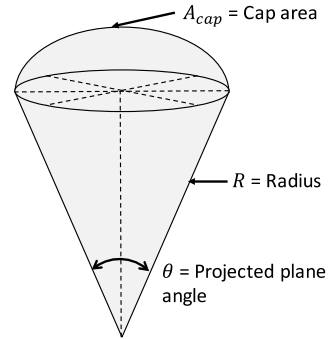


Fig. 4. Schematic drawing of the concept of solid angle and projected plane angle.

The projected plane angle depends upon detector radius, distance between two detectors whilst it is independent to crystal height. The projected plane angle is:

$$\theta(r) [rad] = \tan^{-1}\left(\frac{r_d + r}{D}\right) + \tan^{-1}\left(\frac{r_d - r}{D}\right) \quad (2)$$

where  $r_d$  is a detector radius,  $D$  is a distance. The area averaged projected plane angle ( $\bar{\theta}$ ):

$$\bar{\theta} = \frac{\int_{A_d} \theta(r) dA_d}{\int dA_d} \quad (3)$$

$$\bar{\theta} = \frac{1}{\pi r_d^2} \int_0^{r_d} \left[ \tan^{-1}\left(\frac{r_d + r}{D}\right) + \tan^{-1}\left(\frac{r_d - r}{D}\right) \right] (2\pi r) dr \quad (4)$$

The maximum, minimum, averaged, and half-projected plane angles with detector radius of 2.54 cm and 5.08 cm at different distances are estimated using Eq. (2) to (4) and summarized in

Table 2 and Fig. 5. Projected plane angle becomes narrower when detectors are placed farther. If a distance between two detectors is 0, it can be assumed as one detector and it has a 180° plane angle. In contrast, projected plane angle converges to 0° once detectors are placed away each other.

Table 2 Maximum, minimum, averaged, and half-projected plane angles ( $\gamma$ ) with detector radius of 2.54 and 5.08 cm at five different distances

D [cm]	$r_d$ [cm]	$\theta_{max}$ [deg]	$\theta_{min}$	$\bar{\theta}$	$\gamma = \bar{\theta}/2$
0	2.54	180	180	180	90
	5.08	180	180	180	90
8	2.54	35.2	32.4	33.8	16.9
	5.08	64.8	51.8	58.0	29.0
9.5	2.54	29.9	28.1	29.0	14.5
	5.08	56.3	46.9	51.4	25.7
11	2.54	26.0	24.8	25.4	12.7
	5.08	49.6	42.7	46.0	23.0
$\infty$	2.54	0	0	0	0
	5.08	0	0	0	0

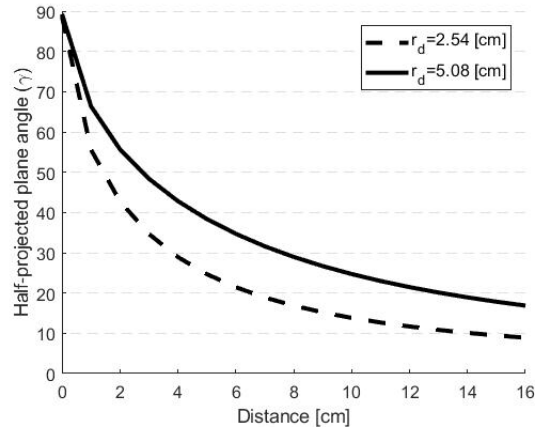


Fig. 5. Estimated half-projected plane angle ( $\gamma$ ) as a function of a detector distance ( $D$ ) with two detector radius,  $r_d = 2.54$  cm (solid), and  $r_d = 5.08$  cm (dashed).

### 3.2. Effective Cosmic Muon Solid Angle Calculation

Intensity of cosmic muon reaching to the Earth surface depends on incident zenith angle. Specifically, it is proportional to the cosine-power of zenith angle,

$$I(\varphi) = I_0(0^\circ) \cos^n \varphi \quad (5)$$

where  $\varphi$  is zenith angle,  $I_0$  is the vertical intensity, and precedent experiments showed  $n \cong 2$  at the sea level [34]. Cosine-squared law is widely used in muon studies and simulations including

GEANT4 [24]. As shown in Fig. 3, two-detectors installation has a limited measurable solid angle. It also has a variance of muon intensity within its solid angle. To calculate the azimuth angular symmetric solid angle corresponding to projected plane angle,

$$\Omega_{cap} = 2\pi \int_0^\gamma \sin \phi d\phi \quad (6)$$

where  $\Omega_{cap}$  is a solid angle of cap indicated in Fig. 4,  $\gamma$  is a half-projected plane angle. Because all detecting materials (crystal, gas, or liquid) have physical dimensions, detector always has its corresponding measurable solid angle. In addition, cosmic muon intensity varies along the zenith angle within measurable solid angle. For example, detection system covers wide measurable angles even a centerline of detectors is placed on at  $\varphi = 0^\circ$ . In other words, the muon intensity is not only changing within the detector's measurable solid angle along the zenith angle, but also changing along the pointing angle. Therefore, cosmic muon effective solid angle (in short effective solid angle,  $\Omega_{eff}$ ) is necessary to be introduced. Zenith angle segments within  $90^\circ$  is defined as:

$$\varphi_i = \frac{\pi i}{2N} \quad (i = 0, 1, 2, \dots, N) \quad (7)$$

where  $\varphi_i$  is  $i^{\text{th}}$  zenith angle and  $N$  is the number of divisions of angle in  $90^\circ$ . In order to take into account both solid angle and zenith angle dependence, effective area is defined in Eq. (8). We define the corresponding effective solid angle as primed effective solid angle ( $\Omega'_{eff}$ ) because it includes the entire azimuth angle at given zenith angle.

$$A_{eff} = 2\pi I_0 \int_{\varphi_i - \gamma}^{\varphi_i + \gamma} I(\phi) \sin \phi d\phi = 2\pi I_0^2 \int_{\varphi_i - \gamma}^{\varphi_i + \gamma} \sin \phi \cos^n \phi d\phi \quad (8)$$

where  $A_{eff}$  is an effective area,  $I_0$  is a vertical cosmic muon intensity. Final expression of Eq. (8) and its corresponding effective solid angle are:

$$A_{eff} = 2\pi I_0^2 \int_{\cos(\varphi_i + \gamma)}^{\cos(\varphi_i - \gamma)} \Phi^n d\Phi = \frac{2\pi I_0^2}{n+1} \cdot [\cos^{n+1}(\varphi_i - \gamma) - \cos^{n+1}(\varphi_i + \gamma)] \quad (9)$$

$$\Omega'_{eff} = \frac{A_{eff}}{I_0^2} = \frac{2\pi}{n+1} \cdot [\cos^{n+1}(\varphi_i - \gamma) - \cos^{n+1}(\varphi_i + \gamma)] \quad (10)$$

where  $\Omega'_{eff}$  is an effective solid angle integrated along entire azimuth angle, and  $\Phi = \cos \phi$ . Since  $A_{eff}$  and  $\Omega'_{eff}$  are the integrated value along entire azimuth angle, a scaling factor is introduced to evaluate area of interest:

$$F(i) = \frac{A_{cap}}{A_{2\pi}(i)} = \frac{1 - \cos \gamma}{\cos(\varphi_i - \gamma) - \cos(\varphi_i + \gamma)} \quad (11)$$

where  $F$  is a scaling factor,  $A_{2\pi}$  is a circular area between  $\varphi \pm \gamma$ . The general expression of effective solid angle is:

$$\Omega_{eff} = \Omega'_{eff} \cdot F(i) = \frac{2\pi}{n+1} (1 - \cos \gamma) \sum_{k=0}^n \cos^k(\varphi_i - \gamma) \cos^{n-k}(\varphi_i + \gamma) \quad (12)$$

When  $n = 2$ ,

$$\Omega_{\text{eff}}|_{n=2} = \left(\frac{2\pi}{3}\right) [\cos^2(\varphi_i - \gamma) + \cos(\varphi_i - \gamma) \cos(\varphi_i + \gamma) + \cos^2(\varphi_i + \gamma)](1 - \cos \gamma) \quad (13)$$

#### 4. Monte Carlo Simulation

In two-detector system, we can estimate incident muon counts by assuming only cosmic muons are energetic enough to be measured at both detectors within a coincidence window size. Not all muons pass through both surfaces, however detected muon must pass both surfaces. Therefore, we generate artificial muon traces on both surfaces and connect two points to retrieve passed muon track. It provides incident angle information and corresponding relative intensity is computed. Hundred muon traces on upper and lower detector surfaces with distance of 8 cm are shown in Fig. 6. Cartesian coordinates of traces on upper and lower surfaces are

$$(x, y, z)_u = (x_m, y_m, D) \quad m = 1, 2, \dots, N \quad (14)$$

$$(x, y, z)_l = (x_n, y_n, 0) \quad n = 1, 2, \dots, N \quad (15)$$

Where  $N$  is number of muon trace on the detector surface. Angles and relative intensity between  $m$  point and  $n$  point are,

$$\theta_{m \rightarrow n} = \cos^{-1} \left( D / \sqrt{\Delta x^2 + \Delta y^2 + D^2} \right) \quad (16)$$

$$I_{m \rightarrow n} = I_0 \cos^2(\theta_{m \rightarrow n}) \quad (17)$$

Where  $\Delta x = x_m - x_n$ ,  $\Delta y = y_m - y_n$ . Therefore, total incident angles and intensities are expressed as  $N \times N$  matrices,

$$\Theta = \begin{bmatrix} \theta_{1 \rightarrow 1} & \theta_{1 \rightarrow 2} & \dots & \theta_{1 \rightarrow N} \\ \theta_{2 \rightarrow 1} & \theta_{2 \rightarrow 2} & \dots & \theta_{2 \rightarrow N} \\ \vdots & \vdots & \dots & \vdots \\ \theta_{N \rightarrow 1} & \theta_{N \rightarrow 2} & \dots & \theta_{N \rightarrow N} \end{bmatrix} \quad (18)$$

$$I = \begin{bmatrix} I_{1 \rightarrow 1} & I_{1 \rightarrow 2} & \dots & I_{1 \rightarrow N} \\ I_{2 \rightarrow 1} & I_{2 \rightarrow 2} & \dots & I_{2 \rightarrow N} \\ \vdots & \vdots & \dots & \vdots \\ I_{N \rightarrow 1} & I_{N \rightarrow 2} & \dots & I_{N \rightarrow N} \end{bmatrix} \quad (19)$$

At different zenith angles ( $\varphi_i$ ), individual muon intensities and mean value are,

$$I_i = I_0 \cos^2(\Theta \pm \varphi_i) \quad (20)$$

$$\bar{I} = \frac{1}{N^2} \sum I_i \quad (21)$$

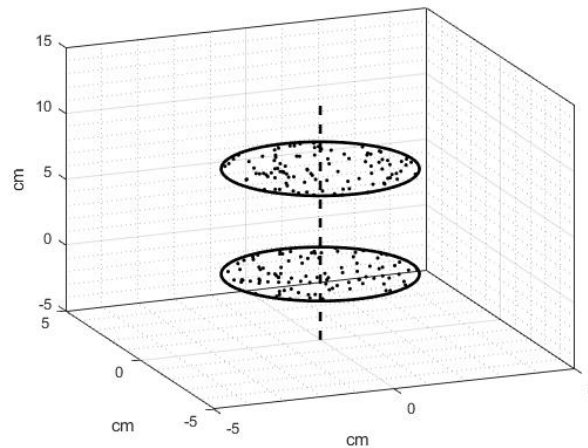


Fig. 6 Arbitrary generated cosmic muon tracks on lower surface of the first (top) detector and upper surface of the second (bottom) detector. Hundred spots are recorded on both surfaces. The centerline (dashed) represents a zenith angle.

## 5. Results and Discussion

Cosmic muons were measured for 24 hours to minimize flux variance upon time in day. In our experiment, seven different zenith angles,  $0^\circ, 15^\circ \dots 75^\circ, 90^\circ$  are considered. In addition, detectors were placed with distance of 8cm, 9.5cm, and 11cm. 9.5 cm represents maximum projected plane angle of  $30^\circ$ . On the other hand, distance of 8cm have overlapped angles while distance of 11cm have angles that cannot be covered. The results of 24-hour measurements, effective solid angle model estimation, Monte Carlo estimation, and cosine-squared law are summarized in Table 2 to Table 4. Normalized counts and estimations are also presented for comparison with the result of cosine-squared law.

For a comparison, experiment results and estimations are normalized. At low zenith angles ( $\varphi \leq 30^\circ$ ), cosine-squared law, effective solid angle model, and Monte Carlo method estimate muon intensity in the error level. However, a cosine-squared law has about 20% relative errors at  $\varphi = 45^\circ$  while the effective solid angle model has about 15% and Monte Carlo method has less than 10%. This trend is enhanced in high zenith angles ( $\varphi \geq 60^\circ$ ). It is known that a cosine-squared law is limited to be applied to high zenith angles and it is shown in our experiment results. Especially, the relative errors constantly exceed 50% and its reliability is no longer valid. Relative errors in effective solid angle model also increase in high zenith angles because muon begins to be detective from the opposite direction. Two models have a similar trend because effective solid angle model is mathematically coupled with cosine-squared model. A concept of solid angle is added to improve the practicality to a measurement and we shows that it estimates muon intensity with less error, especially in high zenith angles. The Monte Carlo method has an agreement with experimental results within a 5% of relative error in nearly all zenith angles. Normalized muon intensities along the zenith angles at different distance (8cm, 9.5cm, and 11cm) estimated by the effective solid angle model, cosine-squared law, and Monte Carlo method with experiment results are shown in Fig. 7. The effective solid angle model

become alike to the cosine-squared model because a detector system becomes a point detector system and a solid angle becomes smaller when two detectors are placed farther.

Muon intensity changes along detector distances are analyzed using the effective solid angle model. Experiment results and model estimations in four zenith angles ( $0^\circ$ ,  $30^\circ$ ,  $60^\circ$ , and  $90^\circ$ ) are shown in Fig. 8. A model estimates a variance of measurable muon intensity by distances at all angles, especially it has a good agreement at  $\varphi = 90^\circ$ . Therefore, it suggests that the effective solid angle model is applicable to the entire zenith angles and various detector distances.

Effective solid angle model is independent to the detector height while it is a function of detector radius and distance. The effective solid angle with a function of a detector radius to distance ( $r_d/D$ ) is shown in Fig. 9. The range  $0 < r_d/D < 5$  is corresponding to  $0.2r_d < D < 20r_d$ , and it represents the practical systemic range. Effective solid angle and  $r_d/D$  has a linear relation at  $r_d/D < 1$ . This relation allows us to facilitate this model to various detector sizes and configurations. A plot approaches to  $\Omega_{\text{eff}} = 2.09$  as a  $r_d/D$  value increases ( $r_d$  increases or  $D$  decreases) because 2.09 rad is an effective solid angle value when a single scintillation crystal has a  $2\pi$  solid angle (hemisphere). In addition,  $\Omega_{\text{eff}}$  converges to 0 when a  $r_d/D$  value decreases because the measurable solid angle approaches to 0. We plotted our experiment results in the figure to verify our model. Our experiment results fall in a range of  $3r_d < D < 5r_d$ . In Fig. 9, experiment results show the linear relation between  $r_d/D$  and  $\Omega_{\text{eff}}$ , which has an agreement with our model estimations.

Table 2 Measured muon counts (24-hours) with errors, normalized Monte Carlo method, effective solid angle model, and cosine-squared law estimations for seven zenith angles at distance 8 cm

Zenith angle ( $\varphi$ )	Counts for 24 hours		Monte Carlo	Effective solid angle		$\cos^2 \varphi$
	Counts	Normalization	Normalization	$\Omega_{\text{eff}}$	Normalization	
0	1929	1.0000 $\pm$ 0.0322	1	0.2484	1	1.000
15	1724	0.8937 $\pm$ 0.0296	0.9368	0.2324	0.9351	0.933
30	1472	0.7631 $\pm$ 0.0264	0.7638	0.1882	0.7577	0.750
45	1192	0.6179 $\pm$ 0.0228	0.5397	0.1280	0.5154	0.500
60	664	0.3442 $\pm$ 0.0155	0.3121	0.0678	0.2731	0.250
75	318	0.1649 $\pm$ 0.0100	0.1467	0.0238	0.0957	0.067
90	156	0.0809 $\pm$ 0.0067	0.0876	0.0153	0.0615	0.000

Table 3 Measured muon counts (24-hours) with errors, normalized Monte Carlo method, effective solid angle model, and cosine-squared law estimations for seven zenith angles at distance 9.5 cm

Zenith angle ( $\varphi$ )	Counts for 24 hours		Monte Carlo	Effective solid angle		$\cos^2 \varphi$
	Counts	Normalization	Normalization	$\Omega_{\text{eff}}$	Normalization	
0	1533	1.0000 $\pm$ 0.0361	1	0.2097	1	1.000
15	1389	0.9061 $\pm$ 0.0336	0.9376	0.1960	0.9347	0.933
30	1206	0.7867 $\pm$ 0.0303	0.7677	0.1586	0.7563	0.750
45	900	0.5871 $\pm$ 0.0247	0.5359	0.1075	0.5126	0.500
60	473	0.3085 $\pm$ 0.0162	0.3042	0.0564	0.2690	0.250
75	213	0.1389 $\pm$ 0.0102	0.1349	0.0190	0.0906	0.067
90	135	0.0881 $\pm$ 0.0079	0.0731	0.0106	0.0506	0.000

Table 4 Measured muon counts (24-hours) with errors, normalized Monte Carlo method, effective solid angle model, and cosine-squared law estimations for seven zenith angles at distance 11 cm

Zenith angle ( $\varphi$ )	Counts for 24 hours		Monte Carlo	Effective solid angle		$\cos^2 \varphi$
	Counts	Normalization	Normalization	$\Omega_{\text{eff}}$	Normalization	
0	1300	1.0000 $\pm$ 0.0392	1	0.1463	1	1.000
15	1160	0.8923 $\pm$ 0.0360	0.9373	0.1367	0.9341	0.933
30	1008	0.7754 $\pm$ 0.0325	0.7650	0.1103	0.7542	0.750
45	742	0.5708 $\pm$ 0.0263	0.5291	0.0744	0.5085	0.500
60	365	0.2808 $\pm$ 0.0166	0.2929	0.0384	0.2627	0.250
75	209	0.1608 $\pm$ 0.0120	0.1197	0.0121	0.0828	0.067
90	114	0.0877 $\pm$ 0.0086	0.0558	0.0050	0.0339	0.000

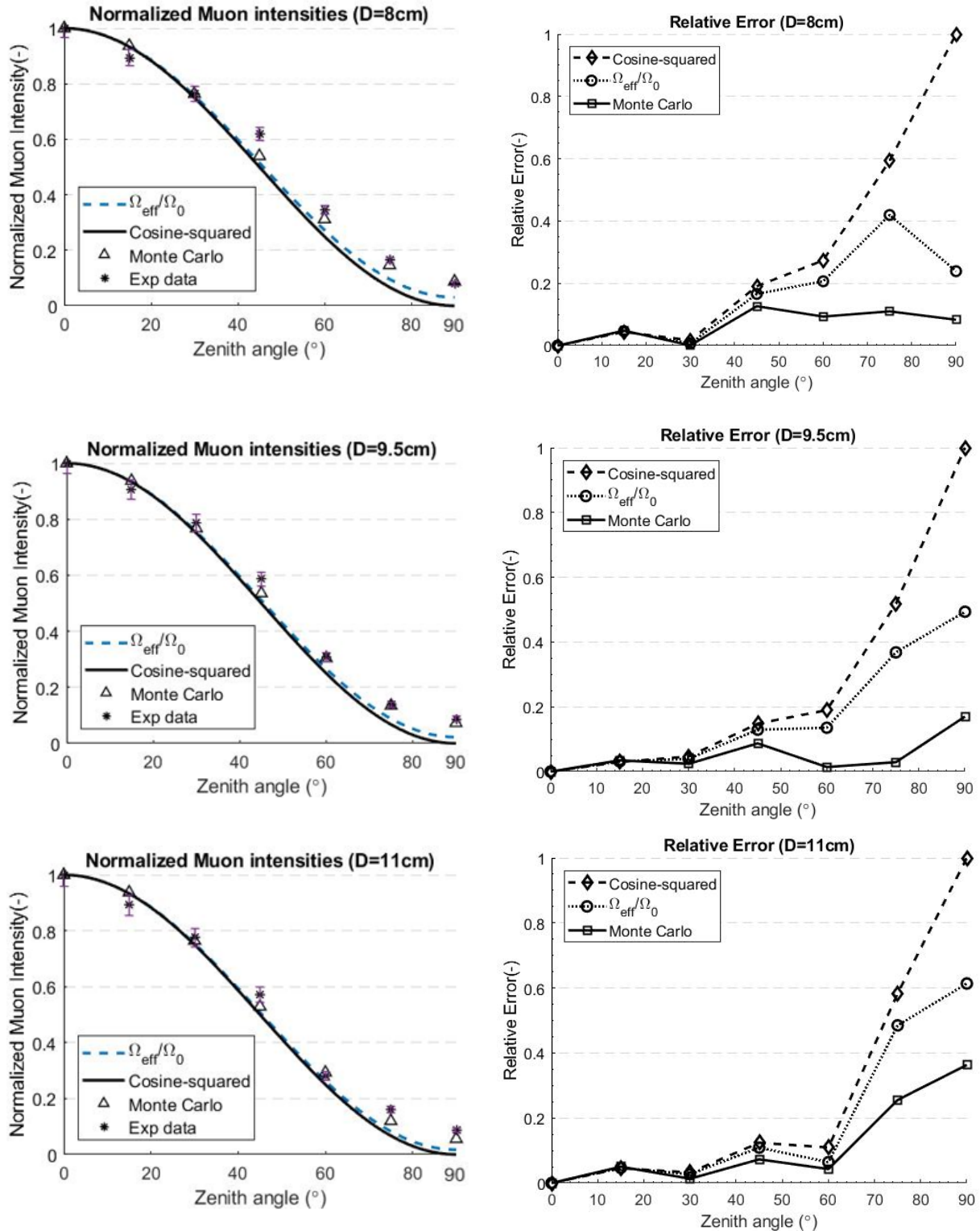


Fig. 7 Normalized muon intensity along the zenith angles estimated by the effective solid angle model (dashed), cosine-squared law (solid), Monte Carlo method (triangle), and experimental data (asterisk) at distances 8cm, 9.5cm, and 11cm (left). Corresponding relative errors with the cosine-squared law (dashed), effective solid angle model (dotted), and Monte Carlo method (solid) along the zenith angles (right).  $\Omega_0$  is an effective solid angle at  $\varphi = 0^\circ$ .

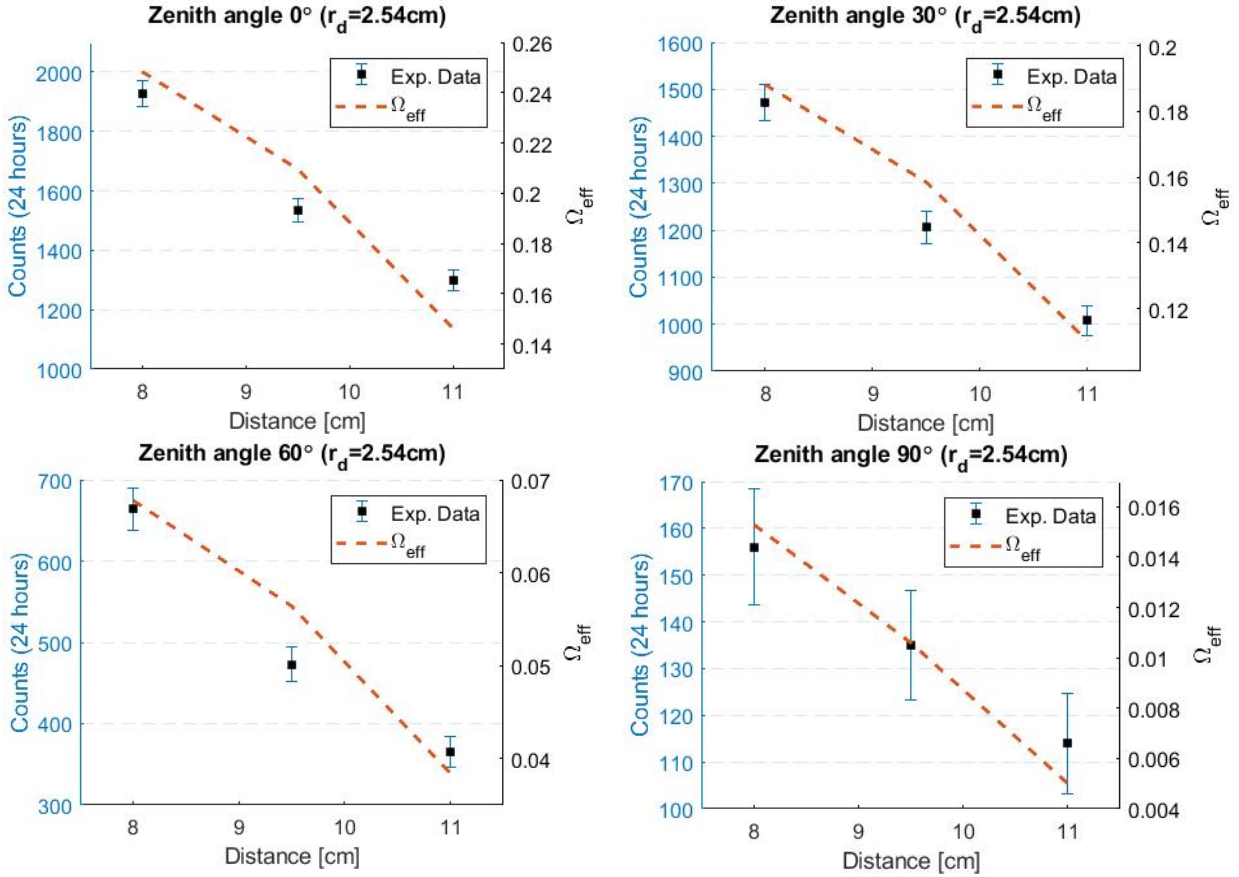


Fig. 8 Relation between measured cosmic muon counts (solid square) and estimated effective solid angles (dashed) at 8cm, 9.5cm, and 11cm when zenith angles are  $0^\circ$ ,  $30^\circ$ ,  $60^\circ$ , and  $90^\circ$

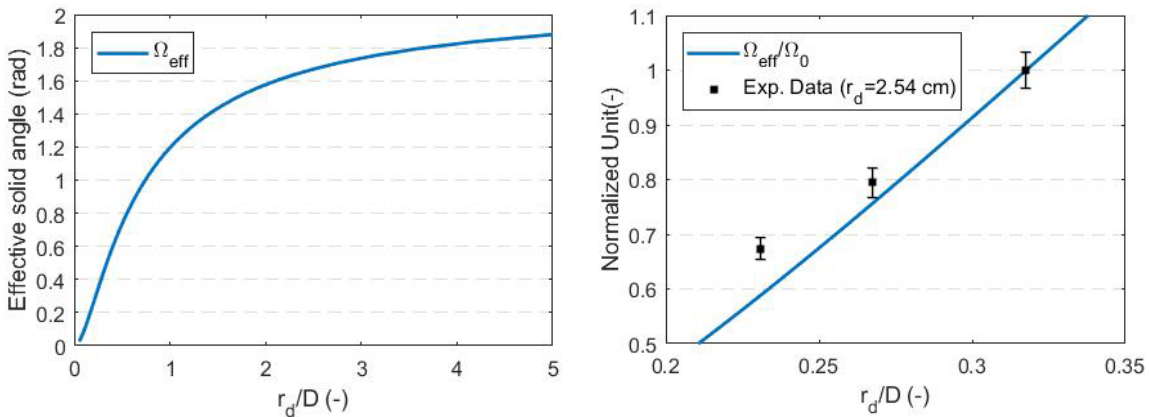


Fig. 9 The effective solid angle as a function of a detector radius to distance ratio ( $r_d/D$ ). A general trend in  $0.2r_d < D < 20r_d$  (left). The effective solid angle approaches to  $\Omega_{\text{eff}} = 2.09$  which represents a single crystal. Normalized effective solid angle and experiment data within a range  $3r_d < D < 5r_d$ .

## 6. Conclusion

In this paper, we discuss the advantages of effective solid angle model and Monte Carlo method for estimating cosmic muon intensity at sea level. The detectable cosmic muon counts in a system vary depending on detector sizes, shape, and setups. The three-dimensional measurable area is termed as a solid angle, and the expected muon intensity variances within a measurable solid angle is denoted as the effective solid angle. In our experiment, two NaI scintillation detectors with a coincidence logic gate are installed to measure cosmic muon intensity at seven zenith angles,  $0^\circ$ ,  $15^\circ$ ...  $75^\circ$ ,  $90^\circ$ . The experiment results are normalized to be compared with a cosine-squared law, effective solid angle model, and Monte Carlo method estimations. The cosine-squared law estimates muon intensity with in an error level in low zenith angles ( $\varphi \leq 30^\circ$ ). However, as it is known, this model is limited to use for high zenith angles ( $\varphi \geq 60^\circ$ ) showing significant relative errors. On the contrary, the effective solid angle model estimates muon intensity with less error than cosine-squared law in all zenith angles. Even this model is improved, it still has a limitation to be used due to the large relative errors in high zenith angles. Monte Carlo method has a good agreement with experiment results in all zenith angles and at all distances.

In addition, the effective solid angle model estimates the muon intensity at different distances between two detectors. We suggest a function of the effective solid angle as a detector radius to distance ratio ( $r_d/D$ ) to apply our model for various sizes and configurations of detection system. They have a linear relation when  $r_d/D < 1$ . Our experimental setup has a range  $0.23 < r_d/D < 0.32$  and results agree with our model estimation showing a linear trend.

Enhanced estimation capability in high zenith angles enables us to use cosmic muon horizontally for muon tomographic applications. In addition, the improved ability to estimate actual cosmic muon count rates reduces the gap between simulation and measurement results. We anticipate this will increase modeling quality in muon detection and imaging. For future works, we will elaborate the model to be applied to complicated detector geometries such as an array of detectors.

## Acknowledgements

This work was supported by the School of Nuclear Engineering, Purdue University.

## References

- [1] P. K. F. Grieder, "Cosmic Rays at Earth," in *Elsevier Science*, Elsevier Science, 2001, p. 1112.
- [2] P. A. Zyla et al. (Particle Data Group), "Review of Particle Physics," *Prog. Theor. Exp. Phys.*, vol. 1, 2020.
- [3] K. N. Borozdin *et al.*, "Radiographic imaging with cosmic-ray muons," *Nature*, vol. 422, no. March, pp. 20–22, 2003.
- [4] D. Schouten, "Muon geotomography : selected case studies," *Philos. Trans. A*, vol. 377, 2018.

- [5] D. Schouten and P. Ledru, "Muon Tomography Applied to a Dense Uranium Deposit at the McArthur River Mine," *J. Geophys. Res. Solid Earth*, no. 123, pp. 8637–8652, 2018.
- [6] K. Morishima *et al.*, "Discovery of a big void in Khufu's Pyramid by observation of cosmic-ray muons," *Nature*, pp. 4–14, 2017.
- [7] S. Buontempo *et al.*, "Perspectives for the radiography of Mt. Vesuvius by cosmic ray muons," *Earth, Planets Sp.*, no. 62, pp. 131–137, 2010.
- [8] L. Del Santo, M.; Catalano, O.; Mineo, T.; Cusumano, G.; Maccarone, M.C.; La Parola, V.; La Rosa, G.; Sottile, G.; Vercellone, S.; Pareschi, G.; Carbone, D.; Zuccarello, "A new technique for probing the internal structure of volcanoes using cosmic-ray muons," *Nucl. Part. Phys. Proc.*, vol. 291–293, pp. 122–125, 2017.
- [9] J. V. P. Baesso, D. Cussans, C. Thomay, "Toward a RPC-based muon tomography system for cargo containers," in *12th WORKSHOP ON RESISTIVE PLATE CHAMBERS AND RELATED DETECTORS*, 2014.
- [10] V. Antonuccio *et al.*, "The Muon Portal Project: Design and construction of a scanning portal based on muon tomography," *Nucl. Inst. Methods Phys. Res. A*, vol. 845, pp. 322–325, 2017.
- [11] B. C. Thomay, J.J. Velthuis, P. Baesso, D. Cussans, P.A.W. Morris, C. Steer and S. Q. and M. S. J. Burns, "A binned clustering algorithm to detect high-Z material using cosmic muons," *J. Instrum.*, 2013.
- [12] C. Burns, Jonathan; Quillin, Steve; Stapleton, Matthew; Steer, "Muon scattering tomography using drift chamber detectors," in *Proceedings of Science, v 0, 2014, Technology and Instrumentation in Particle Physics*, 2014.
- [13] K. Gnanvo, L. V Grasso, M. Hohlmann, J. B. Locke, A. Quintero, and D. Mitra, "Imaging of high-Z material for nuclear contraband detection with a minimal prototype of a muon tomography station based on GEM detectors," *Nucl. Inst. Methods Phys. Res. A*, vol. 652, no. 1, pp. 16–20, 2011.
- [14] C. Frazao, L., Velthuis, J.J., Maddrell-Mander, S., Thomay, "High-resolution imaging of nuclear waste containers with Muon Scattering Tomography," *J. Instrum.*, 2019.
- [15] D. Poulson *et al.*, "Cosmic ray muon computed tomography of spent nuclear fuel in dry storage casks," *Nucl. Inst. Methods Phys. Res. A*, vol. 842, no. September 2016, pp. 48–53, 2017.
- [16] A. Clarkson *et al.*, "GEANT4 simulation of a scintillating-fibre tracker for the cosmic-ray muon tomography of legacy nuclear waste containers," *Nucl. Inst. Methods Phys. Res. A*, vol. 746, pp. 64–73, 2014.
- [17] S. Riggi, V. Antonuccio-delogu, M. Bandieramonte, U. Becciani, and A. Costa, "Muon tomography imaging algorithms for nuclear threat detection inside large volume containers with the Muon Portal detector," *Nucl. Inst. Methods Phys. Res. A*, vol. 728, pp. 59–68, 2013.
- [18] G. Jonkmans, V. N. P. Anghel, C. Jewett, and M. Thompson, "Nuclear waste imaging and spent fuel verification by muon tomography," *Ann. Nucl. Energy*, vol. 53, pp. 267–273, 2013.
- [19] Y. Guangliang *et al.*, "Application of muon tomography to encapsulated nuclear waste," in

*IEEE 12th International Conference on Electronic Measurement & Instruments*, 2015.

- [20] S. Chatzidakis, Z. Liu, J. J. Jarrell, J. M. Scaglione, and J. P. Hayward, "Maximum-a-Posteriori Cosmic Ray Muon Trajectory Estimation with Energy Loss for Muon Tomography Applications," in *IEEE Nuclear Science Symposium and Medical Imaging Conference*, 2017, pp. 20–21.
- [21] S. Chatzidakis, Z. Liu, J. P. Hayward, and J. M. Scaglione, "A generalized muon trajectory estimation algorithm with energy loss for application to muon tomography," *J. Appl. Phys.*, vol. 123, 2018.
- [22] S. Chatzidakis, S. Chrysikopoulou, L. H. Tsoukalas, and M. Carlo, "Developing a cosmic ray muon sampling capability for muon tomography and monitoring applications," *Nucl. Inst. Methods Phys. Res. A*, vol. 804, pp. 33–42, 2015.
- [23] L. Bogdanov, A.G.; Burkhardt, H.; Ivanchenko, V.N.; Kelner, S.R.; Kokoulin, R.P.; Maire, M.; Rybin, A.M.; Urban, "Geant4 simulation of high energy muon interactions," in *IEEE Nuclear Science Symposium Conference Record*, 2004, pp. 2043–2047.
- [24] H. Arslan and M. Bektasoglu, "Geant4 simulation for the zenith angle dependence of cosmic muon intensities at two different geomagnetic locations," *Int. J. Mod. Phys. A*, vol. 28, no. 16, pp. 1–11, 2013.
- [25] H. Burkhardt, "Muon background simulations and Geant4," in *26th Advanced Beam Dynamics Workshop on Nanometer Size Colliding Beams*, 2002.
- [26] C. Schwerdt, "Zenith angle dependence of Cosmic muons," 2018.
- [27] H. M. and K. Cheng, "The Day-night Variation of Cosmic Rays Intensity at Sea Level under the Influence of Meteorological Fronts and Troughs," in *10 Internat. Congress of IRPA*, 2000.
- [28] ORTEC, "Model 276 Photomultiplier Base Operating and Service Manual," Advanced Measurement Technology," 2005.
- [29] Saint-Gobain Crystals, "Integrated Scintillation Detectors," 2018.
- [30] K. Nakamura et al. (Particle Data Group), "The Review of Particle Physics," *J. Phys*, vol. G 37, no. 75021, 2010.
- [31] H. Bichset, "Straggling in thin silicon detectors," *Rev. Mod. Physics. Am. Phys. Soc.*, vol. 60, no. 3, pp. 663–699, 1988.
- [32] AMETEK Inc., "DSPEC 50® and DSPEC 502® Digital Gamma-Ray Spectrometer User's Manual," 2018.
- [33] D. M. Lowder, T. Miller, P. B. Price, A. Westphal, S. W. Barwick, F. Halzen, R. Morse, "Observation of muons using the polar ice cap as a Cerenkov detector," *Nature*, vol. 353, pp. 331–333, 1991.
- [34] C. Y. E. Ho, "Cosmic Ray Muon Detection using NaI Detectors and Plastic Scintillators," University of Virginia.